Food Chemistry: X 23 (2024) 101555

Contents lists available at ScienceDirect

Food Chemistry: X

journal homepage: www.sciencedirect.com/journal/food-chemistry-x

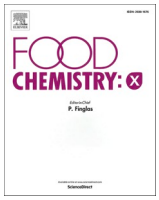

Deep eutectic solvent-functionalized amorphous UiO-66 for efficient extraction and ultrasensitive analysis of perfluoroalkyl substances in infant milk powder

Yaqi Yin, Chen Fan *, Linru Cheng, Yuwei Shan

School of Light Industry Science and Engineering, Beijing Technology and Business University, Beijing 100048, China

ARTICLE INFO

Keywords:
Deep eutectic solvent
Amorphous metal–organic framework
Perfluoroalkyl substance
Milk powder
Dispersive solid-phase extraction

ABSTRACT

In this study, a convenient and effective method for determination of perfluoroalkyl substances (PFASs) in infant formula was developed based on a novel dispersive solid-phase extraction using deep eutectic solvent-functionalized amorphous UiO-66 (DES/aUiO-66) as sorbent. The synthesis of materials could be achieved without the use of complex and environmentally unfriendly procedures. Parameters were systematically investigated to establish a simple, fast, and efficient green pretreatment method. The method demonstrated high sensitivity, good precision, a detection limit of 0.330–0.529 ng·kg^{-1}, and low matrix effects (< 12.8%). The mechanism for this material was elucidated by ab initio molecular dynamics (AIMD) simulations and quantum chemistry calculations. The presence of massive pore structures and collectively synergistic binding sites facilitated affinity adsorption toward PFASs. Finally, this method was applied to the monitoring of PFASs in 10 actual milk powder samples. This groundbreaking approach opens new possibilities for the advancement of analytical techniques and food safety monitoring.

1. Introduction

Per- and polyfluoroalkyl substances (PFASs) are a group of man-made compounds consisting of perfluorinated carbon chains and hydrophilic terminal functional groups. These structural features and strong C—F bonds make them difficult to degrade chemically and biologically while also providing waterproofing, oil resistance, and surface energy reduction effects, making them widely used in various consumer and industrial applications (Van Beijsterveldt et al., 2022). PFASs have a long half-life, can accumulate in humans and other organisms, and have been shown to cause a range of adverse effects, including immunotoxicity, hepatotoxicity, carcinogenicity, and endocrine disruption (Ramirez Carnero et al., 2021). Studies have shown that PFASs can migrate from soil, processing equipment, and packaging into food, making dietary intake the primary route of exposure to PFASs (Abafe, Macheka, & Olowoyo, 2021). In addition, there were ionic interactions between PFASs and proteins that allowed them to bind to β-lactoglobulin in dairy products, making milk an important food source for dietary exposure to PFASs, especially perfluoroalkyl acids (Li et al., 2022). This fact has drawn attention to the monitoring and detection of PFASs in milk. In addition, PFASs and their mixtures may adversely affect early childhood neurodevelopment (Zhou et al., 2023), which might contribute to the manifestation of symptoms associated with attention-deficit/hyperactivity disorder (ADHD) (Kim et al., 2023). Furthermore, exposure to PFASs has been linked to diminished immune responses to childhood vaccinations (Sigvaldsen et al., 2023). Mikolajczyk et al. have studied infant exposure to PFASs in infant formula and baby food and suggested that more sensitive methods should be used given their ultra-trace levels (Mikolajczyk, Warenik-Bany, & Pajurek, 2023).

Mass spectrometry-related techniques are commonly used for their detection in food. Milk powder is a complex sample matrix containing various components such as lipids, sugars, and proteins. These components may interfere with the signal strength of PFASs, thereby affecting the accuracy of quantitative analysis. Therefore, it is necessary to adopt appropriate extraction methods and sample pretreatment steps to ensure the effective extraction of PFASs from milk powder and obtain reliable analytical results. Liquid-liquid extraction (LLE), solid-phase extraction (SPE), dispersive solid-phase extraction (DSPE), and magnetic solid-phase extraction (MSPE) are the most widely used pretreatment technologies in recent years (Guo, Ren, Ji, Yang, & Di, 2022). Among them, DSPE can effectively increase the contact area between the adsorbent and analyte by dispersing the adsorbent throughout the sample

* Corresponding author at: No. 11 Fucheng Road, Beijing Technology and Business University, Beijing 100048, China.
E-mail address: fanchen@btbu.edu.cn (C. Fan).

https://doi.org/10.1016/j.fochx.2024.101555
Received 27 March 2024; Received in revised form 10 June 2024; Accepted 11 June 2024
Available online 13 June 2024
2590-1575/© 2024 The Authors. Published by Elsevier Ltd. This is an open access article under the CC BY-NC license (http://creativecommons.org/licenses/by-nc/4.0/).

extraction solution, shorten the extraction time, and simplify the operation process (Ren, Lu, Han, Qiao, & Yan, 2023). Many widely used adsorbents today are effective only when used in large quantities, which requires a large volume of eluent and additional nitrogen drying procedures, resulting in high costs. Reasonable design of adsorbent types and enhancement of the interaction force between adsorbent and target substance is an effective solution to achieve selective adsorption and efficient extraction (Abad, Masrournia, & Javid, 2024; Cai et al., 2024).

MOFs are considered as potential adsorbents due to their tunable structural properties. However, the regular periodic arrangement of metal ions and organic ligands in traditional crystalline MOFs limits their pore diversity, restricts mass transfer, and conceals metal centers (Wang et al., 2022). Amorphous MOFs are similar in composition to their crystalline counterparts, but lack long-range periodic order in their structure, which results in scale defects, a high degree of disorder, and unique amorphous properties. These additional properties endow them with greater flexibility and a rich pore structure, providing more adsorption sites and channels, which is advantageous for their applications in the field of adsorption. Some functionalized modifiers have been used to enhance the selectivity of materials in complex matrices, such as inorganic acids, carbon nanotubes, and surfactants (Wei et al., 2020). However, these modifiers and material synthesis processes can have detrimental effects on the environment, so there is an urgent need to seek green modifiers and protocols to achieve the goals of sustainable development and eco-friendliness (Liu et al., 2024). Deep eutectic solvents (DESs) are green solvents with good biocompatibility, low toxicity, and biodegradability formed by noncovalent interactions between two or more compounds, which have been used in areas such as electrocatalysts, extraction media, and separations (Li, Dai, Wang, & Row, 2019). Therefore, DESs can be combined with advanced materials to modify their pore surfaces and provide functional groups. Our previous study demonstrated that efficient enrichment and sensitive detection of PFASs with different chain lengths in edible oils can be achieved by rational design of DESs composition (Fan, Wang, Liu, & Cao, 2021).

Based on this background, the aim of this study was to prepare and obtain a novel adsorbent for the detection of trace perfluorocarboxylic acids in infant milk powder samples. This was achieved by functionalizing an amorphous UiO-66 (aUiO-66) consisting of a zirconium metal cation and a terephthalic acid ligand with DES synthesized from acetylpropionic acid and 3-bromobenzeneacetonitrile in different ratios. The DES would induce hetero-halogen interactions, thereby facilitating selective affinity extraction (Fan, Shan, Yin, & Cao, 2023). The fabrication of aUiO-66 was done in the ammonium salts/acetamide-based eutectic mixtures. The parameters affecting the pretreatment process, including the molar ratio of HBD/HBA, the amount of DES/aUiO-66, the extraction time, the type of eluent, and its volume, were optimized by the control-variable method in order to achieve the best extraction efficiency. The mechanism of dispersive solid-phase extraction for this material was elucidated by theoretical simulations and calculations. Finally, the developed method was validated and applied to the analysis of five different chain-length PFCAs in real milk powder samples. To the best of our knowledge, there has been no research on the use of DES-functionalized amorphous MOFs for the analysis of contaminants in food matrices, and this field is still in the exploratory stage. This study provided new ideas and methods for trace analysis of food contaminants and had guiding significance for improving the sensitivity of detection methods.

2. Materials and methods

2.1. Materials and reagents

Terephthalic acid (BDC, 99%), acetamide (99%), zirconium tetrachloride ($ZrCl_4$, 98%), 3-bromophenylacetonitrile (3BP, 98%), diethanolamine hydrochloride (99%), and mass-grade ammonium acetate were purchased from Macklin Biochemical Co., Ltd. (China). Levulinic acid (LA, 98%) was obtained from Heowns Biochemical Technology Co., Ltd. (China). The standards of perfluorocarboxylic acids (PFCAs, >99.0%) were purchased from Sigma-Aldrich (St. Louis, MO), including perfluorobutanoic acid (PFBA), perfluorohexanoic acid (PFHxA), perfluorooctanoic acid (PFOA), perfluorodecanoic acid (PFDA), and perfluorododecanoic acid (PFDoA). The isotopically labeled standard, $^{13}C_8$-PFOA, was obtained from Wellington Laboratories (Guelph, ON, Canada). Mass-grade methanol for liquid chromatography-mass spectrometry (LC-MS) was acquired from Cleman Technology Co., Ltd. (China), and ultrapure water was obtained using a Milli-Q water purification system (Millipore Co., USA).

2.2. Preparation and characterization of DES-functionalized amorphous UiO-66

Amorphous UiO-66 (aUiO-66) was prepared according to the procedure described in our previously published article (Yin, Fan, Shan, & Cheng, 2023). The general procedure is as follows: DES as the reaction medium was obtained by mixing acetamide as HBD and diethanolamine hydrochloride as HBA at a molar ratio of 2:1 at 80 °C, then adding equal molar ratios of $ZrCl_4$ and BDC to the DES solution containing 20% water, and heating and stirring at 100 °C for 5 h to obtain amorphous UiO-66 material. Ideal defect-free UiO-66 was synthesized using *N*,*N*-dimethylformamide (DMF) according to Lillerud's recipe (Shearer et al., 2016). The DES for functionalization of amorphous UiO-66 was prepared by mixing LA as HBD and 3BP as HBA in various molar ratios and heating the mixture in a metal bath until a transparent, uniform liquid was obtained. Then, 5 mg of amorphous UiO-66 was ultrasonically dispersed in 1 mL of ethanol, and 20 μL of the above-prepared DES was added. After ultrasonic mixing for 10 min, the ethanol was dried at 80 °C to produce powdered DES/aUiO-66. Transmission electron microscopy (TEM, JEOL-2000 EX-II) and scanning electron microscopy (SEM, JSM-6700 F) were utilized to observe the morphology and structures of the proposed sorbents. Fourier-transform infrared (FTIR, Nicolet 6700) spectroscopy was conducted within the frequency range of 4000 to 400 cm^{-1}, at a spectral resolution of 2.0 cm^{-1}, using a 1% sample in a KBr pellet. The phases of the amorphous materials were identified through X-ray diffraction (XRD, Rigaku D/MAX-RB) analysis by scanning the diffraction angle (2θ) over the range of 5° to 90° with Cu − Kα radiation. Their specific surface area and porosity characteristics were determined by nitrogen adsorption/desorption isotherm measurements (ASAP 2020 Micromeritics).

2.3. Pretreatment procedure

Infant milk powder (10 g) was weighed into a 50 mL polypropylene centrifuge tube and dissolved in 15 mL of ultrapure water. The internal standard of 2 $\mu g \cdot kg^{-1}$ was added and mixed by sonication. Then 15 mL of acetonitrile was added to precipitate the protein in the sample and centrifuged at 8000 rpm for 10 min at 4 °C. The 12 mL of supernatant was removed with a pipette, 10 mg of DES/aUiO-66 was uniformly dispersed into the sample solution, and it was oscillated and extracted for 15 min. The adsorbent was then separated from the sample solution by high-speed centrifugation at 8000 rpm, and the supernatant was discarded. It was then desorbed by ultrasonic treatment in 200 μL of eluent for 10 min. Finally, the collected eluate was centrifuged, and the supernatant was transferred to a 1.5 mL LC vial with a liner tube for direct LC-MS detection. To minimize errors, all sample extraction procedures were performed three times. To optimize the pretreatment conditions, the conditions after the addition of PFCA standards to the milk were investigated. Five extraction/desorption conditions were investigated, including the amount of adsorbent (5–25 mg), the extraction time (5–30 min), the type of eluents (methanol, acetonitrile, acidified methanol, and alkaline methanol), the proportion of the chosen additive (0.025–0.2%), and eluent volumes (50–400 μL). The selection of eluent type was based on the published literature (Deji et al.,

2022). The specific material preparation and its pretreatment procedure are shown in Fig. 1. The analysis of perfluorocarboxylic acid was based on our published article (Fan et al., 2021).

2.4. Molecular dynamics simulation and quantum chemistry calculation

The geometries of all initial DES materials were fully optimized at the B3LYP-D3(BJ)/def2-TZVP level by the ORCA program system (Version 5.0, https://orcaforum.kofo.mpg.de). Meanwhile, vibrational frequency calculations were performed to confirm the optimized geometries as true minima. The 3-bromophenylacetonitrile/levulinic acid simulation systems with the target analyte (PFBA was selected as the representative compound) contained 55 molecules (HBD: HBA: target = 4:6:1). The initial conformations were initially generated via Packmol (http://m3g.iqm.unicamp.br/packmol), where the solvent molecules were randomly and loosely packed into a cube (4 × 4 × 4 nm). Periodic boundary conditions were implemented for cubic boxes in all directions (box sides: 1.2 Å; tolerance: 2.0 Å). In all cases, long-range Coulomb interactions were calculated using the particle mesh Ewald (PME) method (grid spacing: 0.16 nm; interpolation order: 4). These systems were then classically equilibrated in GROMACS (Version 2022, https://manual.gromacs.org/) for 30 ns under canonical (NVT) and isothermal-isobaric (NPT) ensemble dynamics at 1 atm and 298.15 K. The molecules were treated with the General Amber Force Field (GAFF). The final frame obtained from the classical NPT run was utilized as the input for the ab initio molecular dynamics (AIMD) simulations. The AIMD simulations were carried out in the CP2K package (Version 2024.1, https://www.cp2k.org/) using the TVZP basis set to describe the valence electrons and the Goedecker–Teter–Hutter (GTH) pseudo-potentials for different atom types. Furthermore, the simulations employed the B3LYP exchange-correlation functional with Grimme's DFT-D3 empirical dispersion correction and a time step of 1.0 fs. The system underwent an initial equilibration with AIMD under NPT procedures for 10 ps, followed by a production-level run of 40 ps at 298.15 K held using the V-rescale thermostat. A density cutoff threshold of 520 Ry was implemented. The finest grid level was defined with a multigrid value of 4 and a relative cutoff of 60, employing smoothing techniques for both the electron density and its derivative. The following analyses were conducted by the TRAVIS program (http://www.travis-analyzer.de/). The energy decomposition analysis was performed using the sobEDAw methods (http://sobereva.com/multiwfn/).

2.5. Quality assurance and quality control

The validation of the analytical methods used in this study included linear range, standard curve, recovery, inter-day precision, intra-day precision, matrix effect, limit of detection (LOD), and limit of quantitation (LOQ) to evaluate the applicability of the analytical methods. In all analyses, PFCAs were added to infant milk powder samples at known concentrations, and $^{13}C_8$-PFOA was used as the internal standard for PFCAs. The linear range of the method was evaluated at 9 levels from 0.02 to 40 μg·kg^{-1}, and the correlation coefficient (R^2) was determined by calculating the linear equation of the calibration curve using least squares. The recoveries were determined by adding five selected PFCAs

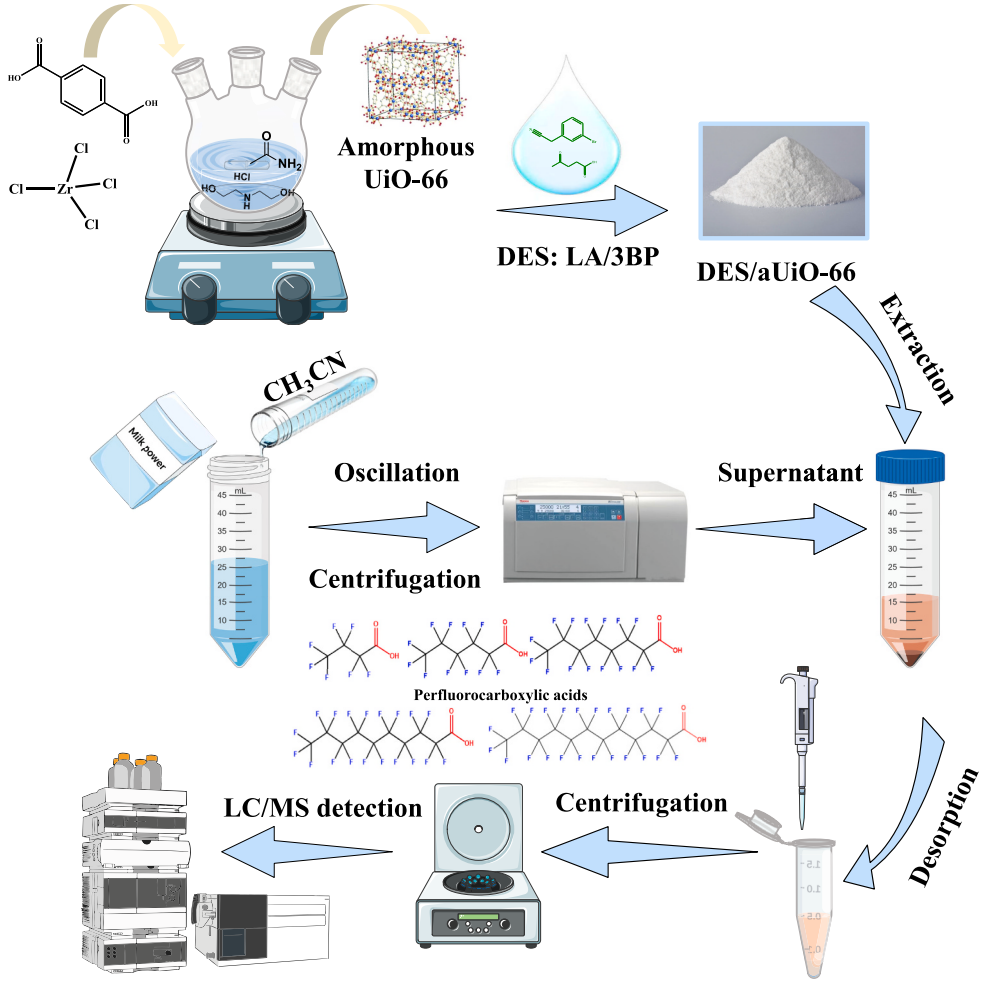

Fig. 1. Pretreatment procedure by using deep eutectic solvent-functionalized amorphous metal-organic framework.

to the milk powder, and the samples were subjected to three replications at two concentration levels (0.02 and 0.2 μg·kg^{-1}). The limit of detection (LOD) and limit of quantification (LOQ) of PFCAs were evaluated by the signal-to-noise ratio of the chromatogram (LOD is S/N = 3, LOQ is S/N = 10). After the addition of 4 μg·kg^{-1} PFCAs to the sample, the entire process was repeated six times in one day and three days, respectively, to evaluate the repeatability of the method. Since the composition of the matrix directly affects the quantification of PFCAs, it is necessary to evaluate the matrix effect. Blank milk powder was pretreated as described in Section 2.3, and PFCAs were added to the blank matrix at a concentration of 0.5 μg·kg^{-1}. The matrix effect was evaluated by comparing the response values of PFCAs added to the blank matrix and the standard solution. To monitor and analyze possible contamination in the workflow, method blanks (i.e., samples prepared from the entire pretreatment process without the addition of infant formula matrix) were also determined, and the results were compared with the LOQ of

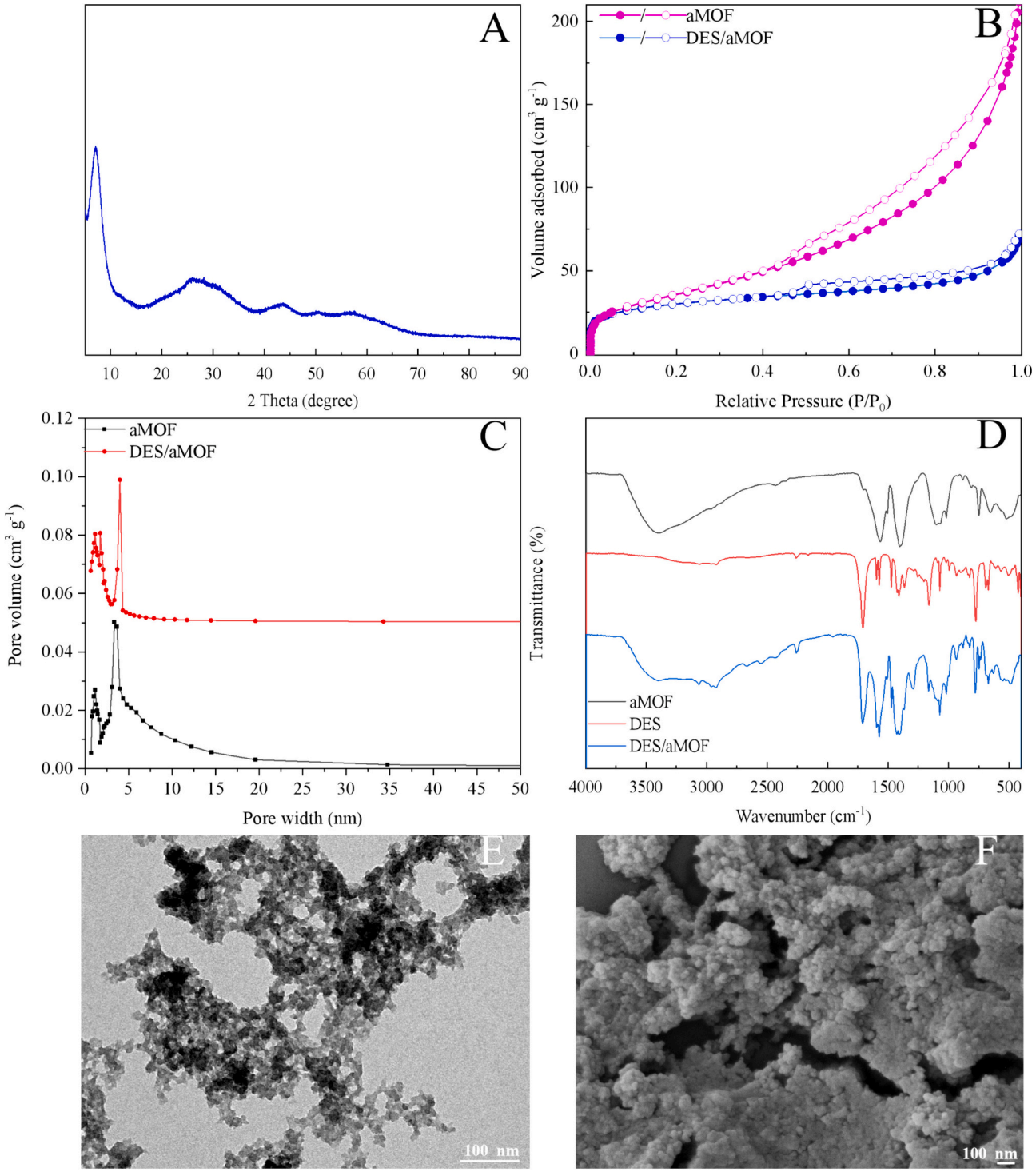

Fig. 2. Characterization of deep eutectic solvent-functionalized amorphous UiO-66 and amorphous UiO-66. (A) XRD pattern of amorphous UiO-66; (B) N_2 adsorption-desorption isotherms; (C) Pore-size distributions; (D) FTIR spectra; (E) TEM image of DES-functionalized amorphous UiO-66; (F) SEM image of DES-functionalized amorphous UiO-66.

PFCAs. All laboratory equipment was thoroughly cleaned with water and organic solvents before use.

3. Results and discussion

3.1. Characterization of DES-functionalized amorphous UiO-66

Fig. 2 (A) shows the XRD pattern of the DES/aUiO-66 material, which has obvious amorphous characteristics. It can be seen that, except for the broad main peak retained by the material at 6.2°, the remaining diffraction peaks are very small in intensity and indistinguishable from each other. This is due to the lack of long-range ordering in DES/aUiO-66 and the inability to form distinct characteristic peaks, which are manifested as broad peaks caused by diffuse scattering (Yin et al., 2023). The N_2 adsorption-desorption curves of aMOF and DES/aMOF are displayed in Fig. 2 (B). Both materials do not have a clear saturation adsorption plateau and show type IV isotherms and H1 hysteresis loops, indicating the presence of mesoporous and irregular pore structures in the materials (Feng, Long, Liu, & Liu, 2022). Further research was conducted on the BET specific surface area and porosity of the adsorbent, and detailed results are listed in Table S1. aMOF has a specific surface area of 130.1 $m^2 \cdot g^{-1}$ and a total pore volume of 0.5954 $cm^3 \cdot g^{-1}$, with 67% mesopores and 32% micropores. DES/aMOF has a specific surface area of 101.4 $m^2 \cdot g^{-1}$ and a total pore volume of 0.4531 $cm^3 \cdot g^{-1}$, with 40% mesopores and 59% micropores. Compared with aMOF, the specific surface area and total pore volume of DES/aMOF decrease, and the number of micropores increases, all due to the introduction of DES into aMOF. Despite the decrease in porosity resulting from the introduction of DES to enhance the selective affinity of the adsorbent materials, it is still superior to the ideal UiO-66, which only possesses limited micropores. From the pore size distribution in Fig. 2 (C), it can be seen that the main pore size of DES/aMOF increases within the mesopore range, indicating that the material still has sufficient pore space, which is conducive to the adsorption of PFCAs by the material.

The results of FT-IR characterization of aMOF, DES, and DES/aMOF are shown in Fig. 2 (D). For primitive aMOF, the broad peak at 3389.65 cm^{-1} correlated with the presence of adsorbed water or hydroxyl groups (Jalali, Ahmadpour, Ghahramaninezhad, & Yasari, 2023). Peaks at 1565 cm^{-1} and 1403 cm^{-1} represented in-phase and out-of-phase tensile vibrations of carboxylic acid groups (Shan, Zhang, Wang, & Liu, 2022). The peak observed at 1101 cm^{-1} corresponded to the tensile vibration of the Zr-OH single bond, demonstrating the binding of the BDC ligand to the Zr node. The peaks at 749, 654, and 523 cm^{-1} were caused by the combination of O—H and benzene ring C—H with Zr—O, which was consistent with previous reports (He et al., 2024). For DES, characteristic bands of LA were observed at 2920.22 cm^{-1} and 1708.72 cm^{-1}, corresponding to stretching vibrations of —OH and C═O, respectively, and the C≡N group vibration peak in 3BP was located at 2259.58 cm^{-1}. In the spectra of DES/aMOF, these different absorption peaks underwent slight shifts. The blue shift of the COOH/COO- group vibration peak in aMOF indicated the possibility of hydrogen bonding between DES and the material. After the functionalization of DES, the broad band intensity above 3000 cm^{-1} decreased, and new absorption peaks appeared at 1710.81 and 2923.09 cm^{-1} for DES/aMOF, indicating the successful loading of the LA-3BP eutectic system with aUiO-66. The apparent morphology of DES/aUiO-66 was observed by TEM and SEM, as shown in Fig. 2 (E)-(F). It can be seen that this material has nanoscale dimensions, a shape that tends to be spherical, a rough surface, and strong particle aggregation. This is caused by strong interactions between molecules, and the highly curved edges of their surfaces also show relatively high reactivity (Mokhtari, Khosrowshahi, Farajzadeh, Nemati, & Mogaddam, 2022).

3.2. Comparison of different enrichment materials and effect of HBD/HBA molar ratio

Under the same pretreatment process, the enrichment and adsorption effects of aUiO-66 and DES/aUiO-66 on PFCAs in infant milk powder were evaluated and compared with those of ideal UiO-66 (iUiO-66) and DES/ideal UiO-66 (DES/iUiO-66). The initial extraction conditions were as follows: the HBD/HBA molar ratio of DES was 5:5, the adsorbent dosage was 5 mg, the adsorption time was 30 min, and 200 μL of acetonitrile served as the elution solvent. From the recovery of each PFCA in Fig. 3 (A), it is known that there is a significant difference in the enrichment ability between functionalized and non-functionalized MOFs, and the enrichment ability of aUiO-66 is significantly better than that of iUiO-66. aUiO-66 had a higher adsorption capacity than iUiO-66, which may be due to interactions, including physical adsorption of aUiO-66 and chemical adsorption between PFCAs and adsorbents (Yin, Fan, Cheng, & Shan, 2024). However, the recoveries of PFCAs in milk powder by pristine UiO-66 were limited, which would be due to the rapid saturation of nonspecific adsorption sites (Li et al., 2021). After functionalization with DES, the materials showed higher adsorption capacity for PFCAs, which could be attributed to the formation of new adsorption sites by encapsulating DES on the surface of aUiO-66 (Liu et al., 2019). Therefore, the material's extraction capacity for five different types of PFCAs can be improved by modifying the amorphous material using DES functionalization. The molar ratio of HBD/HBA in DES is crucial for its physical properties and the extraction efficiency of the target substance. The effect of different molar ratios of HBD/HBA (3:7, 4:6, 5:5, 6:4, 7:3) on the extraction of PFCAs from milk powder by DES/aUiO-66 was investigated. As shown in Fig. 3 (B), the adsorption effect of DES/aUiO-66 on PFCAs reaches its maximum at 4:6, and the recovery is significantly better than other ratios. This may be attributed to the oxygen-containing functional groups in DES forming hydrogen bonds or dipole-dipole interactions with PFCAs to enhance the extraction performance (Eid et al., 2023), which will be clarified in the following section.

3.3. Optimization of extraction conditions for DES-functionalized amorphous UiO-66

A significant factor influencing extraction efficiency is the number of adsorption sites, which correlates with the amount of adsorbent. In this experiment, the effects of 5, 10, 15, 20, and 25 mg DES/aUiO-66 dosage on sample recovery were investigated (Fig. 3 (C)) to determine the optimal adsorbent dosage. The findings demonstrated that the recovery of PFCAs in infant milk powder reached its maximum value when the adsorbent dosage was increased to 10 mg, and the recovery gradually decreased when the adsorbent dosage was further increased. This could be explained by the fact that increasing the adsorbent dose resulted in more active sites, which improved the adsorption efficiency of PFCAs. When excessive amounts were used, the particles were more prone to agglomeration, and it was difficult to effectively elute PFCAs from the material with an eluent, thereby reducing the applicability of the method. It can also be seen from the figure that long-chain PFCAs have a much higher recovery rate than short-chain PFCAs when the dosage of DES/aUiO-66 is low (5 mg). This difference in recovery rate may be due to the higher affinity of long-chain PFCAs for the material (Valencia, Ordonez, Sadmani, Reinhart, & Chang, 2023), which allowed them to take the lead in competitive adsorption on the material when there were fewer adsorption sites. Short-chain targets (PFBA, PFHxA, PFOA) were more easily desorbed by limited eluents when the dosage of DES/aUiO-66 was high (> 10 mg), and their recoveries did not change significantly with the amount of adsorbent used. As a result, the ideal adsorbent dosage for subsequent experiments was 10 mg of DES/aUiO-66.

In the extraction process, the DES/aMOF particles were uniformly dispersed in the sample solution by oscillatory adsorption using an oscillator, which could effectively increase the contact area between the

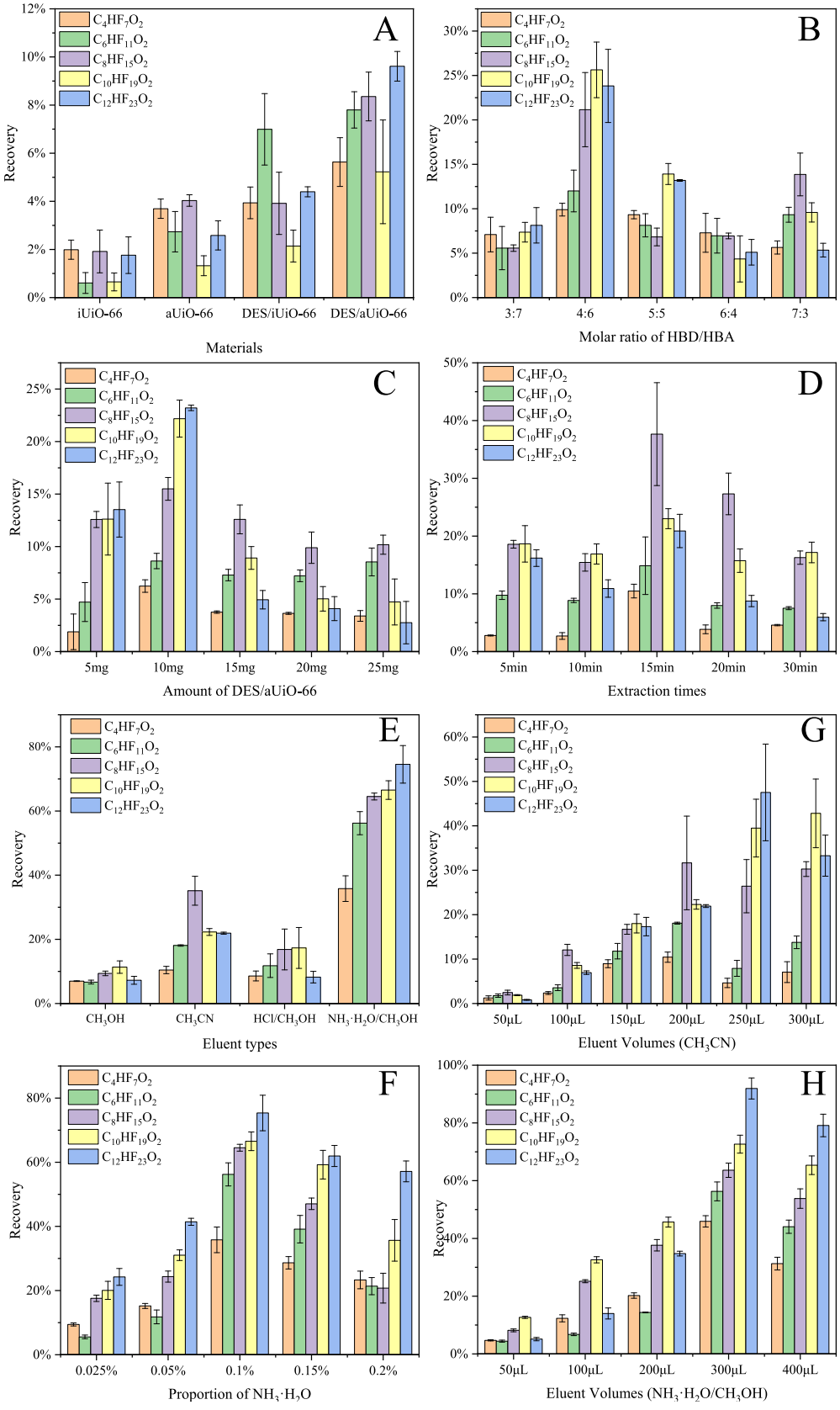

Fig. 3. (A) Effects of different extraction materials on the extraction efficiency of perfluorocarboxylic acids, including iUiO-66 (ideal UiO-66), aUiO-66 (amorphous UiO-66), DES/iUiO-66 (DES-functionalized ideal UiO-66), and DES/aUiO-66 (DES-functionalized amorphous UiO-66); (B) Effects of different molar ratios of HBD/HBA on the extraction efficiency of perfluorocarboxylic acids; Optimization of extraction conditions. (C) Amount of DES-functionalized amorphous UiO-66; (D) Extraction time; Optimization of desorption conditions. (E) Type of eluents; (F) Volume proportions of $NH_3 \bullet H_2O$ in CH_3OH; (G) Elution volumes of CH_3CN; (H) Eluent volumes of 0.1% $NH_3 \bullet H_2O/CH_3OH$.

material and the sample. It took time for the analyte to transfer from the solution to the material, so the contact time between the adsorbent and the solution was another important parameter to optimize. The effect of adsorption time on extraction efficiency was investigated by varying the oscillation time (5–30 min). The results of Fig. 3 (D) show that the recoveries of PFCAs reach their maximum when the adsorption is carried out for 15 min. If the oscillation time is too long, the extracted PFCAs will desorb from the DES/aMOF surface, which reduces the efficiency of the method. Therefore, 15 min was chosen as the best extraction time in the following experiment.

3.4. Optimization of desorption conditions

An appropriate eluent can efficiently desorb analytes from the adsorbent surface, which is a critical element in determining the concentration of the up-sample assay. Four types of eluents were tested for their influence on the extraction effect: methanol (CH_3OH), acetonitrile (CH_3CN), $NH_3{\bullet}H_2O/CH_3OH$, and HCl/CH_3OH. As shown in Fig. 3 (E), the recoveries of the five target substances were significantly improved when $NH_3{\bullet}H_2O/CH_3OH$ was used as the eluent. The reason for the low elution effect of a single solvent might be that different interaction forces were involved in the adsorption process between PFCAs and adsorbents. However, the addition of a small amount of $NH_3{\bullet}H_2O$ disrupted the hydrogen bonding and electrostatic interactions between the PFCAs and adsorbents, which was beneficial for the elution of the acidic target substances. The other potential explanation for this phenomenon could be attributed to the diminished hydrophobic interaction between PFASs and the adsorbent in an alkaline environment, resulting in easier elution of the PFASs (Deji et al., 2022). Conversely, the hydrophobic interaction between PFASs and the adsorbent would be intensified in an acidic environment. Therefore, $NH_3{\bullet}H_2O$ can be employed as a suitable elution solvent to further investigate the influence of different ammonia addition ratios on the extraction efficiency. Fig. 3 (F) illustrates that the addition of 0.1% $NH_3{\bullet}H_2O$ to CH_3OH resulted in the maximum recovery of the target. Further increasing the ammonia content resulted in a decrease in recovery. Therefore, the 0.1% $NH_3{\bullet}H_2O/CH_3OH$ solution was selected as the elution solvent.

In this method, the volume of the eluent should be sufficient to uniformly disperse the material and effectively desorb PFCAs. Besides, the volume of the eluent should not be too high to ensure a good enrichment factor and achieve a lower detection limit. We evaluated the influence of 0.1% $NH_3{\bullet}H_2O/CH_3OH$ and pure acetonitrile (the most used one in the reported works) as eluents on the recovery in the concentration range of 50–400 μL and 50–300 μL, and the experimental results are shown in Fig. 3 (G) and Fig. 3 (H). The results showed that the elution effect of 0.1% $NH_3{\bullet}H_2O/CH_3OH$ was much better than that of acetonitrile solution. The recoveries of PFCAs increased steadily as the volume of the 0.1% $NH_3{\bullet}H_2O/CH_3OH$ solution increased between 50 and 300 μL, and began to decline after the eluent exceeded 300 μL. For subsequent tests, 300 μL was chosen as the eluent volume.

3.5. Mechanism

AIMD simulations were utilized to precisely investigate the origin of the extraction characteristics of materials. The use of AIMD does not require the specification of a force field, making it a suitable method for studying functional materials with different chemical compositions. AIMD simulations have the ability to provide an accurate and unbiased investigation of the processes of interest. The initial peak of each radial distribution function (RDF) was identified as the defining factor for potential hydrogen bonds, facilitating the determination of interatomic (donor-acceptor) interaction distance and strength. The resulting atomic interaction sites were methodically arranged into a connection matrix (cmat), where interactions were assigned a color code based on the peak distance and height of the RDF (Fig. 4 (A)). The analysis of the connection matrix allows the identification of atom pairs with noteworthy interactions, including hydrogen bonding. Regarding the 3-bromophenylacetonitrile and levulinic acid pairs, the interactions are mainly developed by the –COOH group in the levulinic acid (H5 atom) with the cyano group in the 3-bromophenylacetonitrile through its N atom. After the addition of the target molecule, the trimers are formed by the H atom of the carboxyl group in PFBA with the N atom of the

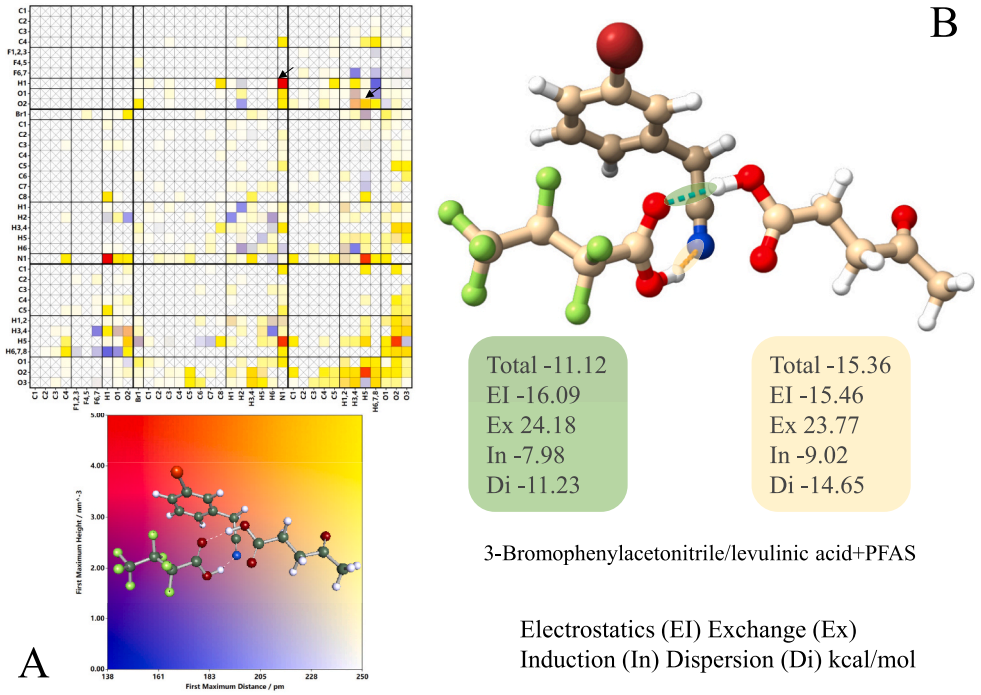

Fig. 4. (A) Connection matrix analysis of the perfluorocarboxylic acid in 3-bromophenylacetonitrile/levulinic acid eutectic solvent (4:6, molar ratio). Row stands for hydrogen bond acceptors; Column represents hydrogen bond donors; The color in each square: the intensity and distance of the first maximum in the corresponding radial distribution functions (RDF); (B) Binding energy and physical components of the corresponding binding energy at B3LYP-D3(BJ)/def2-TZVP level.

cyano group in 3-bromophenylacetonitrile, as well as the O atom of the carboxyl group in PFBA with the H atom of the carboxyl group in levulinic acid. The graph also suggests the possible presence of weak unsymmetrical or hetero-halogen F···Br interactions as well as homo-association of HBD. To compare the strength of these non-covalent interactions, different binding energy (BE) values were obtained at the B3LYP-D3(BJ)/def2-TZVP level (Fig. 4 (B)). The BE between PFBA and levulinic acid within the trimer is determined to be −11.12 kcal·mol^{-1}, with electrostatic interactions (−16.09 kcal·mol^{-1}) playing a major role in the formation of the bond. Additionally, the BE value between PFBA and 3-bromophenylacetonitrile within the trimer system exhibits a larger magnitude (−15.36 kcal·mol^{-1}) and is also dominated by electrostatic interactions (−15.46 kcal·mol^{-1}). In the non-covalent interactions between PFBA and 3-bromophenylacetonitrile, the dispersion energy component cannot be overlooked (−14.65 kcal·mol^{-1}), as it is almost comparable to the electrostatic interactions. The proposed eutectic system provides selectivity for the target analyte to a certain extent. Furthermore, the PFAS adsorption on amorphous UiO-66 is driven by synergistic capture effects according to our previously published research: (1) coordinative bonding interaction (acid/base) between the carboxyl group termini of the targets and the Zr center of the amorphous materials; (2) the fluorine of PFASs interacts with the π-electrons of the aromatic compounds through CF-π; (3) the hydrogen bonding interaction between = O of PFCA and -OH of the massively exposed protonated BDC ligand; (4) hydrophobic interaction (Yin et al., 2024). The presence of multiple types of interactions and the flexible structure of the DES/amorphous UiO-66 nanocomposite material significantly increased the exposure of functional groups to the target analytes and facilitated the subsequent DSPE process.

3.6. Method validation

The linear range, recovery, reproducibility, limit of quantification (LOQ), limit of detection (LOD), and matrix effect of the method were validated under optimized pretreatment conditions, and the results are shown in Table 1. After extraction, working solutions containing a range of concentrations of PFCAs were analyzed, and standard curves were plotted. According to the fitting results, the five PFCAs have acceptable linearity in the range of 0.02–40 μg·kg^{-1}, with $R^2 \geq 0.998$. Next, the recovery rates of the spiked samples were measured at two concentrations (0.02 and 0.2 μg·kg^{-1}), with results ranging from 69% to 118% and a relative standard deviation (RSD) of 0.23–6.28%, indicating that the method had good accuracy and precision. In addition, the limit of detection (LOD, S/N = 3) of the method was 0.330–0.529 ng·kg^{-1} and the limit of quantification (LOQ, S/N = 10) was 0.549–0.882 ng·kg^{-1}, confirming that this method has ultrasensitive analysis of PFCAs. Repeatability tests were conducted at a concentration of 4 μg·kg^{-1} for each PFCA, and the accuracy of the procedure was examined in both intra-day (n = 6) and inter-day (n = 6) scenarios, with an assessment based on the relative standard deviation (RSD). Based on the calculated results, the RSD ranged from 1.26% to 5.56%, suggesting good reproducibility of the method. Overall, the DES/aMOF-DSPE method has good linearity, a low detection limit, and high precision for the detection of PFCAs in milk powder samples. Other compounds in milk powder samples may affect the signal intensity of the mass spectra, causing a difference in the peak areas of PFCAs in matrix and standard solutions, and therefore, this matrix effect needs to be evaluated. In this study, a single-site extraction method was validated at a concentration level of 0.5 μg·kg^{-1} of each PFCA, and each sample was repeated three times. The results showed a weak matrix effect, with values ranging from 1.1 to 12.8%, indicating that the method can accurately determine PFCAs in milk powder.

3.7. Analysis of different milk powders

We used the proposed DES/aMOF-DSPE-based method to verify its suitability for the detection of PFCAs in 10 commercially available infant milk powder samples under optimized extraction conditions. Fig. 5 shows the typical chromatograms of spiked milk powder after pretreatment (top) and unspiked milk powder after pretreatment (bottom). Each sample was analyzed three times to ensure reproducibility. As shown in Table 2, all 10 milk powder samples showed the presence of PFCAs. Among them, the detection values of short-chain PFCAs were higher, while the detection values and rates of long-chain PFCAs were lower. The concentration of each target analyte in infant milk powder samples of different brands varied, with the concentration range of PFBA from 4 to 28 ng·kg^{-1}, PFHxA from 1 to 19 ng·kg^{-1}, PFOA from 2 to 28 ng·kg^{-1}, PFDA from 2 to 11 ng·kg^{-1} (the target substance was not detected in one of the samples), and PFDoA from 2 to 7 ng·kg^{-1} (not detected in three samples). The above assays are generally consistent with published literature (Zhang et al., 2020). Since PFCAs have been shown to bind to proteins, it is possible that PFCAs may accumulate in samples with high protein content. As a control, no significant target peaks were found in the chromatograms of deionized water without DES/aMOF treatment and with DES/aMOF treatment (Fig. S1). These results suggest that the developed assay can effectively extract and sensitively detect trace PFCAs in milk powder samples. In 2020, the European Food Safety Authority revised its previous scientific opinions

Table 1
Quality analytical parameters of the entire method under optimum conditions.

Compounds	Linearity range[a] (μg·kg^{-1})	Calibration equation[b]	R^2	Spiked concentrations (μg·kg^{-1})				Reproducibility		LOD[c] (ng·kg^{-1})	LOQ[c] (ng·kg^{-1})	Matrix effect
				0.02		0.2		Intra-day	Inter-day			
				Recovery (%)	RSD (%, n = 3)	Recovery (%)	RSD (%, n = 3)	RSD (%, n = 6)	RSD (%, n = 6)			
PFBA	0.02–40	y = 1540.6× + 1605.2	0.9985	70	0.26	70	0.56	4.26	5.56	0.525	0.859	12.8%
PFHxA	0.02–40	y = 1874.3× + 1484.9	0.9995	69	5.05	75	0.47	4.28	4.59	0.529	0.882	8.3%
PFOA	0.02–40	y = 2012.1× + 2470.7	0.9978	86	0.23	89	0.45	1.26	2.41	0.330	0.549	1.1%
PFDA	0.02–40	y = 2348.3× + 2116.7	0.9980	94	6.28	110	2.24	2.13	1.95	0.357	0.595	3.1%
PFDoA	0.02–40	y = 2528.5× + 1840.1	0.9996	118	1.26	94	2.30	1.68	1.90	0.456	0.763	4.9%

[a] Linear range was determined by spiked milk power samples with different concentration level of PFCAs after the pretreatment.
[b] Calibration equation was determined by spiked milk power samples with different concentration level of PFCAs after the pretreatment.
[c] Limit of detection (LOD): the concentration of targets, whose peak area was three times the area of the blank noise (S/N ≥ 3); Limit of quantification (LOQ): the concentration of targets, whose peak area was ten times the area of the blank noise (S/N ≥ 10).

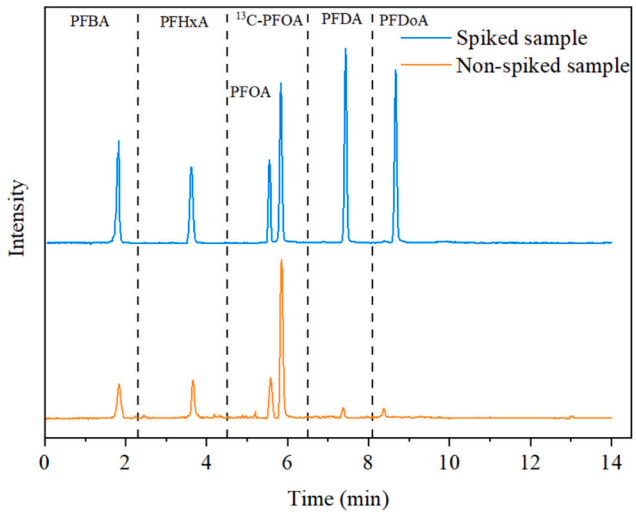

Fig. 5. The typical chromatograms of perfluorocarboxylic acids obtained by the method. Spiked milk power sample 0.2 μg·kg^{-1} after pretreatment (above); non-spiked milk power sample after pretreatment (below).

Table 2
Determination of target PFCA in actual milk powder samples (ng·kg^{-1}).

Sample [a]	PFBA	PFHxA	PFOA	PFDA	PFDoA	∑
Sample 1	22.25 ± 3.26	15.98 ± 2.23	16.69 ± 3.22	3.11 ± 0.60	5.11 ± 0.44	62.14 ± 9.75
Sample 2	28.13 ± 0.84	6.44 ± 0.97	28.65 ± 0.75	4.78 ± 0.43	ND	68.00 ± 2.99
Sample 3	3.54 ± 0.77	1.38 ± 0.24	13.64 ± 0.80	ND	1.62 ± 0.29	20.20 ± 2.13
Sample 4	12.92 ± 2.47	3.37 ± 0.33	6.74 ± 0.54	2.83 ± 0.26	3.12 ± 0.94	28.98 ± 4.55
Sample 5	13.36 ± 0.57	1.52 ± 0.17	17.22 ± 0.87	1.77 ± 0.21	7.61 ± 0.20	41.48 ± 2.02
Sample 6	21.45 ± 1.70	18.56 ± 0.90	3.13 ± 0.68	3.58 ± 0.27	ND	46.72 ± 3.54
Sample 7	3.94 ± 0.51	0.94 ± 0.07	12.21 ± 0.69	2.36 ± 0.80	5.79 ± 0.30	25.24 ± 2.37
Sample 8	10.81 ± 1.61	5.53 ± 0.44	9.06 ± 0.61	5.61 ± 0.35	6.54 ± 0.28	37.55 ± 3.30
Sample 9	10.28 ± 0.87	4.42 ± 0.50	7.20 ± 0.82	11.39 ± 0.61	ND	33.29 ± 2.80
Sample 10	10.53 ± 0.51	4.48 ± 0.42	2.24 ± 0.19	10.89 ± 0.48	2.10 ± 0.07	30.25 ± 1.67

ND: not detectable.
[a] Samples 1–8 were milk powders, and samples 9–10 were goat milk powders.

and established a new tolerable weekly intake for PFASs, setting the threshold at 4.4 ng/kg$_{bw}$ per week for a combined sum of four PFASs. Furthermore, under Regulation (EU) 2022/2388, individual maximum contaminant levels were defined for these four PFASs, including their cumulative concentrations, across various food categories such as eggs and seafood, meat, and offal. However, the current regulatory framework does not specify permissible concentration limits for PFASs in infant milk powder. Research has indicated associations between the nutrition sources of infants at four months and the PFAS concentrations in their dried blood spots, revealing that formula-fed or mixed-fed infants exhibit higher PFAS levels compared to those who are exclusively breastfed, thereby underscoring a potential health risk (Heinsberg et al., 2024).

3.8. Comparison with other methods

The LLE method has become increasingly obsolete due to its well-documented shortcomings, including significant solvent consumption and high sample requirements. Despite these recognized drawbacks, LLE continues to be utilized by many researchers for the extraction of PFASs (Ogunbiyi et al., 2023). In contrast to traditional LLE, SPE has shown distinct advantages, including an improved ability to isolate target analytes from interfering components, reduced extraction timeframes, and diminished organic solvent consumption. However, SPE faces its own challenges, as the elution of long-chain PFASs is more difficult than that of their shorter-chain counterparts due to their reduced polarity. Integrating environmentally friendly techniques or employing alternative, straightforward sample pretreatment methods could successfully mitigate potential interferences, enhance the enrichment factor, and effectively isolate the analyte (Dhiman & Ansari, 2024). DES/aMOF has not yet been used as an adsorbent for dispersive solid-phase extraction of PFCAs in milk powder. Several representative methods for the detection of PFCAs in milk were compared, including the characteristics of adsorbent dosage, extraction time, eluent volume, reproducibility, and LOD, and the results are shown in Table 3.

The findings show that the DES/aMOF-DSPE approach developed in this work is more straightforward, faster, and more effective than previous reports. This can be attributed to the high pore volume and excellent selective adsorption of the DES/aMOF adsorbent material, which provides evidence that the adsorbent was more efficient and rapid. Due to its lower LOD than most other technologies and higher enrichment coefficient in the eluent, this method has good sensitivity. Furthermore, although the LOD of the developed method was comparable to that of Fe_3O_4@COF (covalent organic framework), the current method achieved superior reproducibility and precision, showing that it is more accurate and reliable. It is evident from the literature that extraction methods using commercial adsorbents involve cumbersome steps, a long cycle time, and the need for repeated drying and redissolution. In comparison, the DES/aMOF-DSPE method does not require a complex adsorbent synthesis process, nor does it involve the use of harmful solvents during the synthesis process. It has advantages such as environmental friendliness, lower cost, a simple pretreatment process, fast extraction speed, and accurate and ultrasensitive analysis, which has good potential for application in the detection of trace PFCAs in milk or milk powder. Future research endeavors should consider prioritizing the elimination of the centrifugation step and the seamless integration of automated processes with a variety of analytical instruments. Furthermore, it is essential to expand the scope to include PFASs from other categories.

4. Conclusion

In this study, a new material, DES/aUiO-66, was successfully synthesized and used as an adsorbent to dispersedly solid-phase extract PFCAs from infant milk powders. No harmful volatile organic solvents were used throughout the entire material synthesis process. The characterization results demonstrated that DES/aUiO-66 contained the specific functional groups provided by DES in addition to the characteristic properties of aUiO-66, such as a rich pore structure and large specific surface area. Therefore, it is endowed with excellent selective adsorption properties. Based on these advantages, a method for the detection of analytes in complex food substrates was established. After fine-tuning the sample pretreatment parameters, the optimal extraction conditions were obtained. Interestingly, even a small amount of DES/aUiO-66 (10 mg) could result in an excellent recovery rate (69–118%) in a short extraction time (15 min). The proposed PFASs analysis method exhibited high linearity, low LODs (0.33–0.53 ng·kg^{-1}), good reproducibility (1.26–5.56%), and a low matrix effect (1.1–12.8%), all of which were successfully validated. The mechanism of dispersive solid-phase extraction for this material was elucidated by AIMD simulations and quantum chemistry calculations. The existence of massive pore structures enhanced the accessibility of abundant adsorption sites, and the collectively synergistic binding sites facilitated affinity adsorption toward PFASs. Finally, the method was applied to detect PFCAs in 10

Table 3
Comparison with other pretreatment methods of perfluoroalkyl substances in milk powder and milk.

Samples[c]	Method	Adsorbent		Time (min)	Eluent		Repeatability (%)	Precision (%)	LOD ($ng \cdot kg^{-1}$ or $ng \cdot L^{-1}$)	Reference
		Type	Consumption (mg)		Type	Volume (mL)				
Milk	SPE	Oasis WAX	150	–	NaOH/CH_3OH	6	< 11	< 12	385–2800	Young, South, Begley, Diachenko, & Noonan, 2012
Milk	QuEChERS	C18, PSA, GCB	110	–	HCl/CH_3CN	10	–	1.2–13.1	3–10	Yu et al., 2015
Milk powder	DSPE	C18, PSA	150	–	CH_3CN	10	6.2–13	3–12.2	20–100	He, 2017
Milk	SPME	MMF	–	50	$C_2HF_3O_2$/CH_3CN	0.4	5.3–11	3–11	0.9–12	Huang, Li, Bai, & Huang, 2018
Milk	FM-SPE	Fe_3O_4@COF	20	15	CH_3OH	1.5	0.5–11.8	2.3–11.7	5–50	Zhang et al., 2020
Milk powder	QuEChERS	C18, Oasis HLB	700	10	–	–	5–28	4.6–34	30–60	Abafe et al., 2021
Milk	QuEChERS	Fe_3O_4-SiO_2, ZrO_2, C18	140	5	–	–	< 9.9	< 9.9	4–79	Shi et al., 2024
Milk powder	DSPE	DES/aUiO-66	10	15	$NH_3 \cdot H_2O$/CH_3OH	0.3	1.26–5.56	0.23–6.28	0.33–0.53	This work

Solid-phase extraction (SPE); Dispersive solid phase extraction (DSPE); Quick, easy, cheap, effective, rugged and Safe (QuEChERS); Fluorinated magnetic solid-phase extraction (FM-SPE); Solid-phase microextraction (SMPE); Primary secondary amine (PSA); Graphitized carbon black (GCB); Covalent-organic framework (COF); Deep eutectic solvent (DES); Monolithic fiber (MMF).

milk powder samples with concentrations ranging from 1 to 28 $ng \cdot kg^{-1}$, indicating high sensitivity of the method. In addition, the improved DES/aUiO-66 extraction system was far superior to previously described techniques due to its environmental friendliness, simplicity, speed, and affordability. The utilization of amorphous MOFs and DESs in combination for the analysis of trace PFASs in milk powder presents an innovative approach in the field of green synthesis of functionalized materials and efficient detection of PFASs in food. It is pivotal for developing innovative analytical techniques that minimize the environmental impact of analytical procedures while concurrently improving precision and sensitivity. This pioneering approach has unveiled new avenues for the advancement of trace micropollutant analysis and monitoring in foodstuffs.

CRediT authorship contribution statement

Yaqi Yin: Writing – original draft, Validation, Methodology, Investigation, Formal analysis, Data curation. **Chen Fan:** Writing – review & editing, Writing – original draft, Visualization, Validation, Supervision, Software, Resources, Project administration, Methodology, Investigation, Funding acquisition, Formal analysis, Data curation, Conceptualization. **Linru Cheng:** Data curation. **Yuwei Shan:** Data curation.

Declaration of competing interest

The authors declared that they have no conflicts of interest.

Data availability

The data that has been used is confidential.

Acknowledgment

The authors acknowledge the financial support of this work by the National Natural Science Foundation of China (32102069) and the Science and Technology Program of Beijing Municipal Education Commission (KM2024). Yaqi Yin would like to thank Guangcai Yin and Yun Wang for their care, patience and support over the years.

Appendix A. Supplementary data

Supplementary data to this article can be found online at https://doi.org/10.1016/j.fochx.2024.101555.

References

Abad, M. O. K., Masrournia, M., & Javid, A. (2024). Synthesis of novel MOF-on-MOF composite as a magnetic sorbent to dispersive micro solid phase extraction of benzodiazepine drugs prior to determination with HPLC-UV. *Microchemical Journal, 197*, Article 109797. https://doi.org/10.1016/j.microc.2023.109797

Abafe, O. A., Macheka, L. R., & Olowoyo, J. O. (2021). Confirmatory analysis of per and Polyfluoroalkyl substances in Milk and infant formula using UHPLC-MS/MS. *Molecules, 26*(12). https://doi.org/10.3390/molecules26123664

Cai, Y., Zhang, J., Wen, Y., Zhang, Z., Wang, H., Yang, Y., & Tai, Z. (2024). MOF-525 mixed-matrix membrane-based extraction combined GC–MS for determination of pesticides in root and tuber crops. *Microchemical Journal, 197*, Article 109849. https://doi.org/10.1016/j.microc.2023.109849

Deji, Z., Zhang, X., Liu, P., Wang, X., Abulaiti, K., & Huang, Z. (2022). Electrospun UiO-66-F4/polyacrylonitrile nanofibers for efficient extraction of perfluoroalkyl and polyfluoroalkyl substances in environmental media. *Journal of Hazardous Materials, 430*, Article 128494. https://doi.org/10.1016/j.jhazmat.2022.128494

Dhiman, S., & Ansari, N. G. (2024). A review on extraction, analytical and rapid detection techniques of per /poly fluoro alkyl substances in different matrices. *Microchemical Journal, 196*, Article 109667. https://doi.org/10.1016/j.microc.2023.109667

Eid, S., Darwish, A. S., Lemaoui, T., Banat, F., Hasan, S. W., & Alnashef, I. M. (2023). Multicriteria design of novel natural hydrophobic deep eutectic solvents for the extraction of perfluoroalkyl acids using COSMO-RS. *Journal of Molecular Liquids, 382*. https://doi.org/10.1016/j.molliq.2023.121996

Fan, C., Shan, Y., Yin, Y., & Cao, X. (2023). Special structural and dynamical interplay of cyano-based novel deep eutectic solvents. *New Journal of Chemistry, 47*(11), 5356–5366. https://doi.org/10.1039/D2NJ05274A

Fan, C., Wang, H., Liu, Y., & Cao, X. (2021). New deep eutectic solvent based superparamagnetic nanofluid for determination of perfluoroalkyl substances in edible oils. *Talanta, 228*. https://doi.org/10.1016/j.talanta.2021.122214

Feng, X., Long, R., Liu, C., & Liu, X. (2022). Visible-light-driven removal of tetracycline hydrochloride and microplastics (HDPE) by nano flower hybrid heterojunction NH2-MIL-88B (Fe)/MoS2 via enhanced electron-transfer. *Separation and Purification Technology, 302*. https://doi.org/10.1016/j.seppur.2022.122138

Guo, X., Ren, T., Ji, J., Yang, Y., & Di, X. (2022). An alternative analytical strategy based on QuEChERS and dissolvable layered double hydroxide dispersive micro-solid phase extraction for trace determination of sulfonylurea herbicides in wolfberry by LC-MS/MS. *Food Chemistry, 396*. https://doi.org/10.1016/j.foodchem.2022.133652

He, D. (2017). Simultaneous determination of sixteen industrial pollutants in infant formula milk powder by dispersive solid phase extraction coupled with ultra-high performance liquid chromatography-tandem mass spectrometry. *Analytical Methods, 9*(17), 2561–2569. https://doi.org/10.1039/c7ay00652g

He, T., Wang, Y., Han, R., Li, X., Cui, S., & Yang, J. (2024). Hierarchical porous UiO-66 composites modified by dual competitive strategy for adsorption of oxytetracycline. *Journal of Environmental Chemical Engineering, 12*(1), Article 111662. https://doi.org/10.1016/j.jece.2023.111662

Heinsberg, L. W., Niu, S., Arslanian, K. J., Chen, R., Bedi, M., Unasa-Apelu, F., & Hawley, N. L. (2024). Characterization of per- and polyfluoroalkyl substances (PFAS) concentrations in a community-based sample of infants from Samoa. *Chemosphere, 353*, Article 141527. https://doi.org/10.1016/j.chemosphere.2024.141527

Huang, Y., Li, H., Bai, M., & Huang, X. (2018). Efficient extraction of perfluorocarboxylic acids in complex samples with a monolithic adsorbent combining fluorophilic and anion-exchange interactions. *Analytica Chimica Acta, 1011*, 50–58. https://doi.org/10.1016/j.aca.2018.01.032

Jalali, A., Ahmadpour, A., Ghahramaninezhad, M., & Yasari, E. (2023). Hierarchical nanocomposites derived from UiO-66 framework and zeolite for enhanced CO2 adsorption. *Journal of Environmental Chemical Engineering, 11*(6). https://doi.org/10.1016/j.jece.2023.111294

Kim, J. I., Kim, B. N., Lee, Y. A., Shin, C. H., Hong, Y.-C., Døssing, L. D., … Lim, Y.-H. (2023). Association between early-childhood exposure to perfluoroalkyl substances and ADHD symptoms: A prospective cohort study. *Science of the Total Environment, 879*, Article 163081. https://doi.org/10.1016/j.scitotenv.2023.163081

Li, G., Dai, Y., Wang, X., & Row, K. (2019). Molecularly imprinted polymers modified by deep eutectic solvents and ionic liquids with two templates for the simultaneous solid-phase extraction of Fucoidan and Laminarin from marine kelp. *Analytical Letters, 52*(3), 511–525. https://doi.org/10.1080/00032719.2018.1471697

Li, M., Liu, Y., Li, F., Shen, C., Kaneti, Y. V., Yamauchi, Y., & Wang, C. (2021). Defect-rich hierarchical porous UiO-66(Zr) for tunable phosphate removal. *Environmental Science & Technology, 55*(19), 13209–13218. https://doi.org/10.1021/acs.est.1c01723

Li, Y., Yao, J., Zhang, J., Pan, Y., Dai, J., Ji, C., & Tang, J. (2022). First report on the bioaccumulation and trophic transfer of Perfluoroalkyl ether carboxylic acids in estuarine food web. *Environmental Science & Technology, 56*(10), 6046–6055. https://doi.org/10.1021/acs.est.1c00965

Liu, H., Jiang, L., Lu, M., Liu, G., Li, T., Xu, X., & Xu, D. (2019). Magnetic solid-phase extraction of Pyrethroid pesticides from environmental water samples using deep eutectic solvent-type surfactant modified magnetic Zeolitic Imidazolate Framework-8. *Molecules, 24*(22). https://doi.org/10.3390/molecules24224038

Liu, M., Zhang, L., Yang, R., Cui, H., Li, Y., Li, X., & Huang, H. (2024). Integrating metal-organic framework ZIF-8 with green modifier empowered bacteria with improved bioremediation. *Journal of Hazardous Materials, 461*. https://doi.org/10.1016/j.jhazmat.2023.132475

Mikolajczyk, S., Warenik-Bany, M., & Pajurek, M. (2023). Infant formula and baby food as a source of perfluoroalkyl substances for infants. *Environmental Pollution, 317*. https://doi.org/10.1016/j.envpol.2022.120810

Mokhtari, S., Khosrowshahi, E. M., Farajzadeh, M. A., Nemati, M., & Mogaddam, M. R. A. (2022). A modified quick-easy-cheap-effective-rugged-and-safe method involving carbon nano-onions-based dispersive solid-phase extraction and dispersive liquid-liquid microextraction for pesticides from grapes. *Journal of Separation Science, 45*(18), 3582–3593. https://doi.org/10.1002/jssc.202200124

Ogunbiyi, O. D., Ajiboye, T. O., Omotola, E. O., Oladoye, P. O., Olanrewaju, C. A., & Quinete, N. (2023). Analytical approaches for screening of per- and poly fluoroalkyl substances in food items: A review of recent advances and improvements. *Environmental Pollution, 329*, Article 121705. https://doi.org/10.1016/j.envpol.2023.121705

Ramirez Carnero, A., Lestido-Cardama, A., Vazquez Loureiro, P., Barbosa-Pereira, L., Bernaldo De Quiros, A. R., & Sendon, R. (2021). Presence of Perfluoroalkyl and Polyfluoroalkyl substances (PFAS) in food contact materials (FCM) and its migration to food. *FOODS, 10*(7). https://doi.org/10.3390/foods10071443

Ren, J., Lu, Y., Han, Y., Qiao, F., & Yan, H. (2023). Novel molecularly imprinted phenolic resin-dispersive filter extraction for rapid determination of perfluorooctanoic acid and perfluorooctane sulfonate in milk. *Food Chemistry, 400*. https://doi.org/10.1016/j.foodchem.2022.134062

Shan, Q., Zhang, J., Wang, Y., & Liu, W. (2022). Preparation of ionic liquid-type UiO-66 and its adsorption desulfurization performance. *Fuel, 312*. https://doi.org/10.1016/j.fuel.2021.122945

Shearer, G. C., Vitillo, J. G., Bordiga, S., Svelle, S., Olsbye, U., & Lillerud, K. P. (2016). Functionalizing the defects: Postsynthetic ligand exchange in the metal organic framework UiO-66. *Chemistry of Materials, 28*(20), 7190–7193. https://doi.org/10.1021/acs.chemmater.6b02749

Shi, R., Liu, L., Liu, X., Liu, Z., Liu, J., Wang, J., Di, S., Qi, P., & Wang, X. (2024). Integrated QuEChERS combined with LC–MS/MS for high-throughput analysis of per- and polyfluoroalkyl substances in milk. *Analytical and Bioanalytical Chemistry, 416*(1), 203–214. https://doi.org/10.1007/s00216-023-05008-8

Sigvaldsen, A., Hojsager, F. D., Paarup, H. M., Beck, I. H., Timmermann, C. A. G., Boye, H., … Jensen, T. K. (2023). Early-life exposure to perfluoroalkyl substances and serum antibody concentrations towards common childhood vaccines in 18-month-old children in the Odense child cohort. *Environmental Research, 242*, Article 117814. https://doi.org/10.1016/j.envres.2023.117814

Valencia, A., Ordonez, D., Sadmani, A. H. M. A., Reinhart, D., & Chang, N. (2023). Comparing the removal and fate of long and short chain per- and polyfluoroalkyl substances (PFAS) during surface water treatment via specialty adsorbents. *Journal of Water Process Engineering, 56*. https://doi.org/10.1016/j.jwpe.2023.104345

Van Beijsterveldt, I. A. L. P., Van Zelst, B. D., De Fluiter, K. S., Van den Berg, S. A. A., Van den Steen, M., & Hokken-Koelega, A. C. S. (2022). Poly- and perfluoroalkyl substances (PFAS) exposure through infant feeding in early life. *Environment International, 164*. https://doi.org/10.1016/j.envint.2022.107274

Wang, C., Jiang, A., Liu, X., Yuen Koh, K., Yang, Y., Chen, J. P., & Li, K. (2022). Amorphous metal-organic framework UiO-66-NO2 for removal of oxyanion pollutants: Towards improved performance and effective reusability. *Separation and Purification Technology, 295*, Article 121014. https://doi.org/10.1016/j.seppur.2022.121014

Wei, X., Wang, Y., Chen, J., Xu, F., Liu, Z., He, X., & Zhou, Y. (2020). Adsorption of pharmaceuticals and personal care products by deep eutectic solvents-regulated magnetic metal-organic framework adsorbents: Performance and mechanism. *Chemical Engineering Journal, 392*. https://doi.org/10.1016/j.cej.2020.124808

Yin, Y., Fan, C., Cheng, L., & Shan, Y. (2024). Adsorption of perfluoroalkyl substances on deep eutectic solvent-based amorphous metal-organic framework: Structure and mechanism. *Environmental Research*, 11826. https://doi.org/10.1016/j.envres.2024.118261

Yin, Y., Fan, C., Shan, Y., & Cheng, L. (2023). Fabrication of amorphous metal-organic framework in deep eutectic solvent for boosted organophosphorus pesticide adsorption. *Journal of Environmental Chemical Engineering, 11*(3), Article 109963. https://doi.org/10.1016/j.jece.2023.109963

Young, W. M., South, P., Begley, T. H., Diachenko, G. W., & Noonan, G. O. (2012). Determination of Perfluorochemicals in Cow's Milk using liquid chromatography-tandem mass spectrometry. *Journal of Agricultural and Food Chemistry, 60*(7), 1652–1658. https://doi.org/10.1021/jf204565x

Yu, Y., Xu, D., Lu, M., Zhou, S., Peng, T., Yue, Z., & Zhou, Y. (2015). QuEChERs combined with online interference trapping LC-MS/MS method for the simultaneous determination of 20 Polyfluoroalkane substances in dietary Milk. *Journal of Agricultural and Food Chemistry, 63*(16), 4087–4095. https://doi.org/10.1021/acs.jafc.5b00068

Zhang, M., Li, J., Zhang, C., Wu, Z., Yang, Y., Li, J., & Lin, Z. (2020). In-situ synthesis of fluorinated magnetic covalent organic frameworks for fluorinated magnetic solid-phase extraction of ultratrace perfluorinated compounds from milk. *Journal of Chromatography A, 1615*. https://doi.org/10.1016/j.chroma.2019.460773

Zhou, Y., Li, Q., Wang, P., Li, J., Zhao, W., Zhang, L., … Zhang, Y. (2023). Associations of prenatal PFAS exposure and early childhood neurodevelopment: Evidence from the Shanghai maternal-child pairs cohort. *Environment International, 173*, Article 107850. https://doi.org/10.1016/j.envint.2023.107850